



Accumulation by avalanches as significant contributor to the mass balance of a High Arctic mountain glacier

Bernhard Hynek^{1,2,3}, Daniel Binder^{4,3}, Michele Citterio⁵, Signe Hillerup Larsen⁵, Jakob Abermann^{2,3}, Geert Verhoeven⁶, Elke Ludewig⁷, Wolfgang Schönert^{2,3}

5

¹ Geosphere Austria, Department Climate Impact Research, Vienna, Austria

² Institut für Geographie und Raumforschung, Universität Graz, Austria

³ Austrian Polar Research Institute, Vienna, Austria

⁴ Institute for Geosciences University of Potsdam, Germany

10 ⁵ Geological Survey of Denmark and Greenland, Copenhagen, Denmark

⁶ Department of Prehistoric and Historical Archaeology, Universität Wien, Austria

⁷ Geosphere Austria, Sonnblick Observatory, Rauris, Austria

Correspondence to: B. Hynek (bernhard.hynek@geosphere.at)

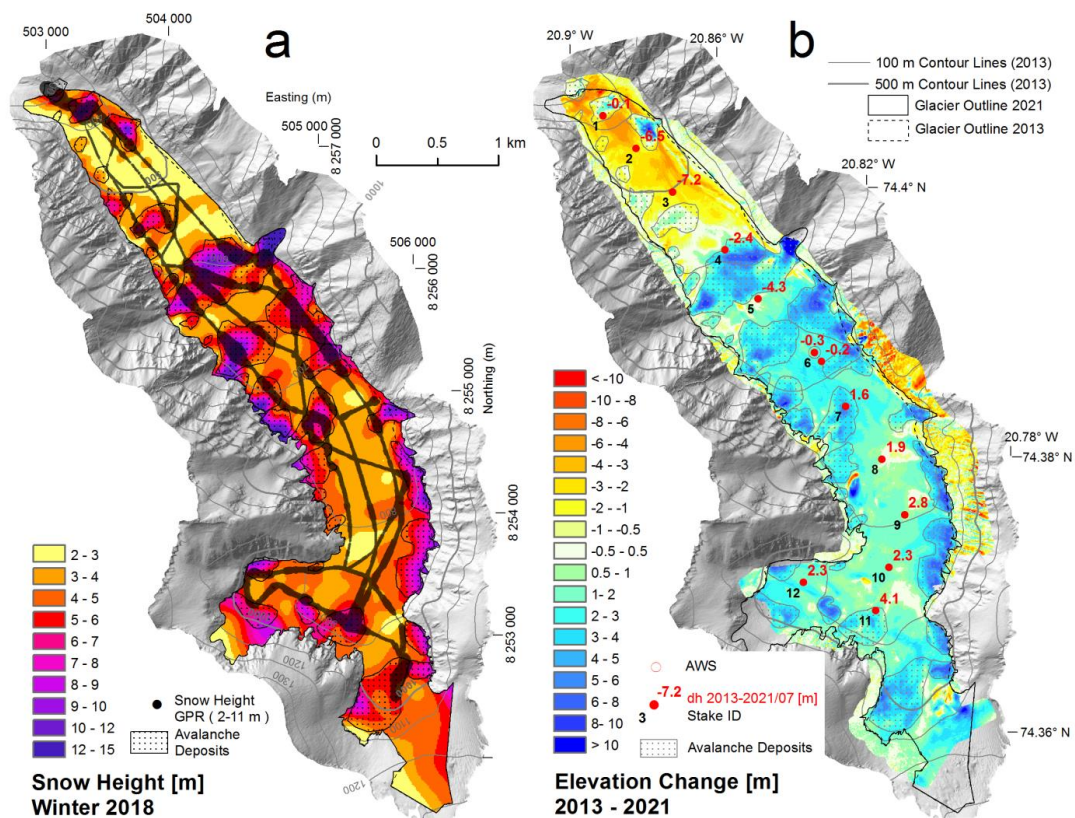
15 *Keywords: UAV; structure from motion photogrammetry; Greenland; glacier mass balance; snow avalanches*

Abstract.

Greenland's peripheral glaciers are losing mass at an accelerated rate and are contributing significantly to sea level rise, but only a few direct observations are available. Here, we use the unique combination of high-resolution remote sensing data and
20 direct mass balance observations to separate and quantify the contribution of a singular avalanche event to the mass balance of Freya Glacier (74.38° N, 20.82° W), a small (5.5 km², 2021) mountain glacier in Northeast Greenland. Elevation changes calculated from repeated photogrammetric surveys on 11th - 18th August 2013 and on 28th - 31st July 2021 range from -11 m to 18 m, with a glacier-wide mean of 1.56 ± 0.10 m (0.85 ± 0.20 m w.e.). Somewhat surprisingly, the geodetic mass balance over
25 the full period of 8 years (2013/14 - 2020/21) is slightly positive, (0.25 ± 0.21 m w.e.). A main imprint of the near decadal mass balance stems from the exceptional (2.5 standard deviations above average) winter mass balance of 2017/18 with 1.85 ± 0.05 m w.e., when in addition to above average precipitation, snow avalanches affected more than one third of the glacier surface and contributed at least 0.31 m w.e. (17%) to the total winter mass balance of 2017/18. We estimate the contribution of
30 avalanches to the accumulated mass balance 2013/14 - 2020/21 as 0.55 m w.e. Without this avalanche event the 8-year mass balance would have been slightly negative, -0.30 m w.e. instead of 0.25 m w.e. Due to a gap in valid observations caused by high accumulation rates and the COVID-19 pandemic the recently reported glacier-wide annual mass balance values now turn out to have a negative bias and demand a thorough reanalysis. Finally, we speculate that the projected future warming increases the likelihood of extreme snowfall events for individual years and thus, may increase the contribution of snow avalanches to the mass balance of mountain glaciers in NE Greenland.



35 **Graphical Abstract.**



40 a) Measured (GPR) and extrapolated snow height in winter 2018 and delineation of avalanche affected areas. b) Elevation Change between 18.8.2013 and 27.7.2021 and stake/AWS locations.



1 Introduction

45 The ice cover of Greenland consists of the Greenland Ice Sheet (GrIS) and ~20 300 peripheral mountain glaciers and ice caps (MGICs) (Rastner et al., 2012; Abermann et al., 2019b). Although Greenland's peripheral glaciers comprise only 4% of the total ice cover of Greenland, their recent mass loss is disproportionately high (11%) in comparison to that of the ice sheet (Khan et al., 2022), confirming the higher sensitivity of MGIC's mass balance to ongoing climate change. During the last 60 years mass loss from MGICs comprise ~ 8% of the world's land ice contribution to sea level rise (Zemp et al., 2019; Frederikse et al., 2020).

50 While total mass loss from the MGICs has accelerated during the last two decades (Hugonnet et al., 2021), the mass loss in Northeast Greenland has decelerated with continued thinning in lower elevations and thickening in higher elevations (Khan et al., 2022). The decelerated mass loss in Northeast Greenland is associated with an increase in precipitation (Hugonnet et al., 2021), whereas the decelerated mass loss of Icelandic and Scandinavian Glaciers is associated with North Atlantic Cooling (Noël et al., 2022).

55 Our knowledge of the individual drivers of mass changes of Greenland's MGICs is limited as direct observations and process studies are scarce. Machguth et al. (2016b) compiled all reported mass balance observations in Greenland and showed that while mass balance observations at the GrIS have increased tenfold, the MGICs are still heavily undersampled despite their topographical and climatological complexity. To our knowledge, currently only 6 out of 20 300 MGICs are monitored in
60 Greenland (Abermann et al., 2019b). Three of them are located on the 2600 km long east coast: Mittivakkat Glacier on Ammassalik Island (65° N) (Yde et al., 2014; Mernild et al., 2013), A.P. Olsen Ice Cap (Citterio and Ahlstrøm, (2010); Larsen et al., (2023) and Freya Glacier (both 74°N near Zackenberg Research Station).

65 The direct or glaciological method (Østrem and Brugmann, 1991; Kaser et al., 2003) to measure the mass balance of a glacier is based on observations of ablation and accumulation at several points on the glacier. These point observations of mass change are then transferred to the whole glacier area, often using additional information like the position of the snowline. However, the specific implementation of this step may vary among glaciers and observers (Zemp et al., 2013) and depending on the number and distribution of the point measurements this introduces a considerable source of error. Annual mass balance measurements are likely to accumulate systematic errors over the years (e.g. Huss et al., 2009), therefore it is recommended to compare and,
70 if necessary, homogenise the annual mass balance time series using decadal volume change measurements (Zemp et al., 2013; Huss et al., 2009; Klug et al., 2018)

75 Interestingly, there are only a few studies on the contribution of snow avalanches to the mass balance of glaciers (Turchaninova et al., 2020) although the importance of this accumulation process seems obvious. Glaciers with considerable accumulation from avalanches are usually associated with high and steep head-walls typical for High Mountain Asia (Laha et al., 2017). The influence of avalanches on the mass balance of some Himalayan glaciers has been quantified by Laha et al. (2017), but to our knowledge snow avalanches have not been shown to have a significant influence on the mass balance of glaciers outside the Himalaya. With increasing temperatures in the Arctic, precipitation is expected to rise, which may lead to heavier single precipitation events as observed over NE Greenland in 2018 (e.g. Schmidt et al., 2019) which can lead to strong avalanche
80 activity (Abermann et al., 2019a).



85 In the last decade, Image-Based 3D surface Modelling (IBM) via hybrid photogrammetric computer vision-based approaches has become commonplace in many academic fields. With photogrammetric methods at their core, these hybrid approaches mainly rely on the computer vision algorithms Structure from Motion (SfM) and Multi-View Stereo (MVS) to digitally extract three-dimensional (3D) surfaces from overlapping images. These 3D surfaces can then be used to produce accurate orthophotographs. Often, such SfM-MVS approaches rely upon terrestrial photographs acquired with consumer-grade cameras (Piermattei et al., 2015; Marcer et al., 2017) or photos obtained via cameras mounted on uncrewed aerial vehicles (UAVs) (e.g. Gindraux et al., 2017; Rossini et al., 2018; Geissler et al., 2021).

90 This study examines the effects of an extraordinary winter accumulation combined with widespread avalanche activity on the multi-year mass balance of an High Arctic mountain glacier. In particular, we quantify the contribution of avalanches to the mass balance 2013/14 – 2020/21 of Freya Glacier (FG) by taking advantage of the unique combination of high-resolution glacier elevation change measurements and distributed seasonal mass balance observations.

95 In the following we calculate IBM-derived elevation changes and deduce the geodetic mass balance of FG between 2013/14 and 2020/21. We delineate snow avalanche deposits of February 2018 on the glacier area and quantify their mass contribution to the winter mass balance 2017/18 and to the multi-year geodetic mass balance. Finally, we compare the geodetic mass balance to the cumulative glaciological mass balance, discuss reasons for the differences and stress the need for a reanalysis of the glaciological record, which suffers from observational gaps caused by travel restrictions during the Covid-19 pandemic and a limited observational network that turned out to be not dense enough to account for the recent spatial variability of surface mass balance on the glacier.

2 Freya Glacier

105 Freya (Freja, Fröya) Glacier (74,38° N, 20.82 W) is a polythermal mountain glacier (Binder et al., 2009) situated on Clavering Island in Northeast Greenland, 10 km southeast of Zackenberg Research Station (Fig. 1). The coastal glacier is oriented towards the Northwest, surrounded by steep ridges on both sides, spans an elevation of 1300 m to 280 m a.s.l. and covers a surface area of 5.5 km² (2021). The glacier was subject to glaciological investigations already in the late 1930s (Ahlmann, 1942, 1946) likely due to its rather good accessibility. During the International Polar Year 2007/2008 a mass balance monitoring programme was initiated (Schöner et al., 2009) which has been ongoing since (Hynek et al., 2014; WGMS, 2013). The current monitoring consists of a stake network, an automatic weather station (AWS) of the PROMICE setup (Fausto et al., 2021) and two high-quality webcams (Hynek et al., 2018). Daily images of two webcams are publicly available via the websites [foto-webcam.eu](https://www.foto-webcam.eu/webcam/freya1/) (110 <https://www.foto-webcam.eu/webcam/freya1/> and <https://www.foto-webcam.eu/webcam/freya2/>) (Freya Glacier Webcam 1, 2023; Freya Glacier Webcam 2, 2023)



115 3 Data and Methods

3.1 Geodetic Survey 2013

Due to the ease of the process and the suitable topography, SfM-MVS-based image-based 3D surface modelling was the optimal choice for generating a DEM of Freya Glacier during the 2013 field campaign. No UAV was available, but the ridges around the glacier offered useful natural viewpoints for a ground-based survey. Between 11th and 18th August 2013 we took oblique
120 overlapping photographs of the glacier surface from about 450 locations on the slopes on both sides of the glacier using a Nikon D7100 digital single lens reflex camera with a 20 mm fixed lens. Simultaneously with the image acquisition, we surveyed ~100 natural Ground Control Points (GCPs) using a differential GNSS (Global Navigation Satellite System) receiver (Fig. 2). For postprocessing of the survey, a temporary GNSS reference station was established on stable rock next to the glacier. We surveyed the upper part of the glacier on the 11th and 12th of August 2013, when the glacier surface was almost snow free. A
125 snowfall event on 14th August followed by a period of low visibility marked the end of the melt season. On 18th August 2013, we surveyed the lower part of the glacier. Surface ablation between the survey dates was below 0.15 m and was partly compensated by an average fresh snow height of 0.10 m.

3.2 Geodetic Survey 2021

The second high-resolution DEM used in this study stems from 2021. On 29th and 31st July 2021, we used a UAV (DJI Phantom
130 4 RTK) to obtain an overlapping image series of the glacier surface. On 29th July, we photographed 80% of the glacier surface (lower part) and finished the drone flights on 31st of July. On 28th and 29th of July 2021, we surveyed ~100 mainly artificial GCPs on the glacier surface using a differential GNSS receiver and a base station that was put up at the same location as in 2013 (Fig. 3). During the survey, surface ablation between 28th and 31st July was less than 0.2 m. Surface ablation between 29th July and the end of the ablation season on 5th September was 0.8 m (mean value of all stakes). Table 1 lists the main
135 characteristics of both photogrammetric surveys.

3.3 GNSS and IBM workflow

GNSS raw logs containing the GCPs and the UAV trajectory were post-processed using the reference station next to the glacier. Coordinates were transformed into UTM coordinate reference system (zone 27N, epsg:32627) and to orthometric heights (egm96). For the accuracy assessment of the surface reconstruction, one subset of the GCPs was used to reference the generated
140 3D model (control points), and another subset was used to validate the 3D model (independent check points). All GCPs were used to reference the final DEM. GCPs that were not clearly visible in the imagery were used for elevation validation of the final DEM output. The workflow of the DEM and orthophoto generation followed the classical SfM process (e.g. Rossini et al., 2018) using Agisoft Metashape (AgiSoft LLC, 2023). Due to the different surface texture (snow covered vs snow free) of the lower and upper 2013 imagery, both parts of the glaciers were processed independently.

145 3.4 Elevation Changes and Geodetic mass balance

Elevation Changes 2013-2021 were calculated by DEM differencing in 1 m planar resolution. Georeferencing of the two final DEMs is based on all respective GCPs, a co-registraion of the DEMs (Nuth and Kääb, 2011) was not carried out, as the overlapping area on stable terrain outside the glacier is too small. To convert the elevation changes into a geodetic mass balance, we used spatially distributed density estimates: the density of ice ($910 \pm 10 \text{ kg/m}^3$) for areas with elevation losses and an
150 estimated firn/snow density of $600 \pm 100 \text{ kg/m}^3$ for areas with elevation gain. In 2013 the survey was very close to the end of the ablation season, in 2021 an adjustment between the survey date and the end of the ablation season in 2021 was calculated based on 10 ablation stake readings.



3.5 Quantifying the influence of avalanches on the mass balance

If feasible, a ground-penetrating radar (GPR) snow survey is done in spring to determine the spatial distribution of winter snow depths for FG. In spring 2018, an extended GPR snow survey with a total distance of 27 km was carried out to also probe the still visible avalanche deposits. Strong increase of snow heights along those GPR tracks, photos from fieldwork and from the two webcams were used to delineate the 2018 avalanche deposits. The GPR snow depth data set was sampled down to 10 m point distance and then interpolated using a spline function to receive a grid of glacier-wide snow heights. To estimate the contribution by avalanches to the winter mass balance of 2018, we calculated spatial averages of the snow height grid on avalanche affected areas and on avalanche free areas. To transfer snow heights into snow water equivalent, we used the same bulk snow density for the whole glacier. To simulate the geodetic mass balance without avalanches, we averaged elevation changes of avalanche-free areas on 25 m wide elevation bins and extrapolated those values to the whole glacier area of the individual elevation bins. By comparing the result to the actual mean elevation change, we get an estimate of the influence of snow avalanches on the multi-year geodetic mass balance.

3.6 Glaciological mass balance

3.6.1 Winter mass balance

Due to logistical challenges in accessing FG with a snow mobile, the number of snow height observations varies considerably from year to year. Distributed winter snow height is measured either by 40 - 150 manual snow depth probings, or by a 800 MHz GPR snow survey of several km in length. In April 2018, the snow depth data coverage was rather dense and bulk snow density was measured next to the AWS at an elevation of 680 m. To get a regular grid of snow height, a spline function was fitted to the data. Winter mass balance was calculated as a spatial average over the whole glacier area.

3.6.2 Annual mass balance

Since 2016 fieldwork takes place only once a year in spring. Annual mass balance is measured at 11 ablation stakes, which usually stick out of the winter snow. However, in spring 2018 and 2019 only two stakes were found, and in 2020 and 2021 there was no spring field trip due to the travel restrictions caused by the COVID-19 pandemic. For those years the annual glacier wide mass balance was estimated using a statistical relationship between the ablation at the AWS (index stake), the accumulation area ratio (AAR), and the glacier wide mass balance. In July 2021 and in spring 2022, most stakes were found again and could be measured.

180



4. Results

4.1 DEM and orthophoto 2013

The shaded relief of the 2013 DEM (Fig. 3a) shows a high level of detail. Only a few artefacts are visible in the middle part of the glacier and in the uppermost part, where the distance of the photo points to the glacier surface is high and the angle towards the glacier surface is acute. Especially the middle part of the glacier is covered poorly, the GCPs there (Fig 3a, set 3) could not be identified in the images and were used to check only the vertical accuracy of the DEM in that area (Table 2). The orthophoto shows the almost snow free conditions in the upper part of the glacier and the new snow on the lower part of the glacier (Fig. 3b). The surface reconstruction covers the whole glacier area and the adjacent ridges. As all GPCs are on the glacier surface, the accuracy of the surface reconstruction is expected to drop significantly in the adjacent ridges. The accuracy of the surface reconstruction expressed as RMSE at the check points is significantly lower than the RMSE at the control points, where especially the lateral accuracy is lower than the vertical accuracy (Table 2).

4.2 DEM and orthophoto 2021

The shaded relief of the 2021 DEM (Fig. 4a) shows a much higher level of detail due to the better measurement geometry and resolution. The ground sample density (Table 1) and the accuracy of the surface reconstruction (Table 2) of the 2021 survey are both higher than for the 2013 survey. However, only 95% of the glacier surface is reconstructed and the DEM does not extend much to the adjacent ridges, as UAV battery supply was limited during the fieldwork. Remnants of the 2018 avalanche deposits are still visible in the orthophoto (Fig. 4b) on the lower and middle part of the glacier, while the upper part was still covered by slush and winter snow.

4.3 Elevation Changes and Geodetic Mass Balance

Elevation changes in 1 m resolution (Fig. 5b) were calculated for 95% of the glacier area, missing only some smaller parts in the upper accumulation zone of the glacier. Elevation changes for these areas were calculated by fitting a spline function to the elevation changes in the surroundings, to avoid a bias in the geodetic mass balance. Elevation changes show a high spatial variability. Surface lowering is observed on 20% of the glacier surface, dominating elevations below 600 m a.s.l., and reaching a minimum of -11 m in the lowest part of the glacier. Above 600 m a.s.l. elevation changes are mainly positive. At the centerline of the glacier, elevation gains are mainly smaller than 2 m. In several distinct areas predominantly along both sides of the glacier, elevation gains are up to several meters with a maximum of 17 m. These areas coincide with potential avalanche depositions from larger side valleys. The mean elevation change 08/2013 – 07/2021 for the total glacier area is 1.56 ± 0.10 m. Main uncertainty is introduced by ablation during the survey, unmeasured areas, and the uncertainty in the delineation of the glacier surface area. Converting this volume change into a mass change – and hereby introducing another uncertainty using a density assumption - we obtain the specific geodetic mass balance 08/2013 – 07/2021 as $b_{\text{geod}} = 0.85 \pm 0.20$ m w.e. To get the geodetic mass balance for the full mass balance year of 2013/14-2020/21 we have to account for additional mass losses during August 2021. Based on the reading of 10 stakes we estimate this mass change to be $-0.60 \text{ m} \pm 0.05$ m w.e., which makes the total 8-year geodetic mass balance 2013/14 – 2020/21 slightly positive: $b_{\text{geod.8y}} = 0.25 \pm 0.21$ m w.e.

4.4 2018 avalanche deposition

While remnants of small snow avalanches are visible also in other years, they usually are not visible during spring field surveys. However, in spring 2018 signs of large avalanche deposits were visible all over the glacier. Especially in the middle part of the glacier several large avalanches originating from the tributary valleys on both sides of the glacier covered large parts of the



glacier. In April 2018 avalanche deposits were found on 36% of the glacier area. Individual GPR-derived snow heights ranged
220 from 2.2 m up to 12.1 m, with a median snow height of 4.0 m. The distribution of snow height and the delineation of avalanche
influenced areas is shown in Fig. 5a. Area averaged values of snow height on the entire glacier is 4.8 m, on avalanche deposits
6.2 m, and on areas with no avalanches 4.0 m. The snow height contribution from avalanches averaged over the whole glacier
is 0.8 m. Mean snow density at the snow pit next to the AWS at stake 6 was 385 kg/m³. Assuming the same bulk snow density
225 everywhere on the glacier, the specific mass balance contribution of avalanches is 0.31 m w.e., which is 17% of the total winter
mass balance of 1.85 ± 0.05 m w.e. This can be seen as a lower limit as the avalanche snow likely has a higher snow density
than the undisturbed snowcover in the middle of the glacier, where the snow density measurement was carried out (Sovilla et
al., 2001). If we assume an increase in bulk snow density of 10% due to compaction and overburden pressure within the
avalanche deposits, the mass contribution of avalanches would be 0.39 m w.e., being 20% of a winter mass balance of 1.93
m w.e. Remnants of the avalanches are still visible on the glacier surface 3 years after the anomalous year (Fig. 4b and Fig. 6c,e)
230 and have altered local surface mass balance significantly at stake 1 (-0.1 m), stake 4 (-2.4 m) and stake 11 (+4.1 m) (Fig 5b).

4.5 Influence of avalanches on the elevation changes

The altitudinal distribution of the elevation changes (dh, Fig. 7) are plotted for all grid cells and as a spatial average on 25 m
altitudinal bins. Without the contribution from avalanches the mean elevation change would have been 0.71 m (instead of 1.56
235 m). The geodetic mass balance would have been 0.30 m w.e. (instead of 0.85 m w.e.). Hence, snow avalanches contributed 0.55
m w.e. to the multiyear mass balance. This value is significantly larger as the lower boundary of the contribution of avalanches
to the winter mass balance of 2018 0.31 m w.e.

4.6 Glaciological mass balance 2013/14- 2020/21

The reported timeseries of winter and annual mass balances (World Glacier Monitoring Service, 2022) of FG are shown in Fig.
240 8. Prior to the first DEM in 2013 mass balances were more negative, especially the mass balance of 2013 was so far the most
negative on record. While annual mass balances 2014-2016 are based on more than 10 point observations, the annual mass
balances of 2017 – 2021 are based on only 1-2 point observations and therefore have a large uncertainty. However, all 11 stakes
were recovered in 2021, the cumulative point mass balance 2013/08 – 2021/07 is shown in Fig.5b. Especially stake 1 and stake
4 are influenced by avalanches and show reduced ablation rates. The cumulative glaciological mass balance 2013/14-2020/21
245 is -1.2 ± 0.4 m w.e. The bias to the geodetic mass balance is -1.4 m w.e. or -0.18 ma^{-1} w.e.



5 Discussion

A major uncertainty in the geodetic mass balance is introduced by the density assumption. Measurements of firn density in
250 Greenland (Braithwaite et al., 1994; Vandecrux et al., 2018) have shown, that the firn density varies a lot depending on the
amount of accumulation and melt at a specific site and particularly on the formation of ice layers by percolating meltwater.
Machguth et al. (2016a) showed, that firn loses a part of its capacity to store water after building near surface ice layers during
strong melt events. Huss (2013) has shown in a model experiment, that a conversion factor between elevation change and mass
change of $850 \pm 60 \text{ kgm}^{-3}$ is appropriate for a wide range of conditions over longer time periods, but that this factor can vary
255 significantly on timescales below 10 years. On FG, high accumulation rates by avalanches generated thick and possibly dense
firn layers with high potential of meltwater retention and refreezing. However it is difficult to constrain the snow density of the
avalanche snow without a measurement. (Li et al., 2021) and (Sovilla et al., 2001) observed that the snow density of avalanche
deposits might be two or three times higher than the undisturbed snowpack at the time of the avalanche release date. Refreezing
of meltwater has already been suspected to play an important role in the mass balance of FG (Ahlmann, 1946) and has been
260 observed qualitatively during fieldwork in 2021. The bright glacier surfaces, that are the remnants of the 2018 avalanches looked
like snow, but proved to be as hard as ice. Based on these considerations, we estimate the mean firn density in July 2021 on FG
as $600 \pm 100 \text{ kgm}^{-3}$.

The cumulative glaciological mass balance carries uncertainties for several reasons: In some years only one or two point
265 observations were available, thus, the glacier-wide mass balance was estimated using a statistical relationship based on the mass
balance at the AWS (stake 6). However, this statistical relationship might have changed, because stake 6 was not influenced by
avalanches and due to a general shift of rather negative mass balances before 2013 and rather positive mass balances after 2013,
which surely has changed the vertical distribution of the mass balance. Another likely reason for the bias between the
glaciological and geodetic mass balance is the internal accumulation by percolation of meltwater and refreezing within deeper
270 layers of the avalanche deposits. This process is generally difficult to measure; in the case of FG it was not feasible to measure
firn density due to logistical reasons. A thorough reanalysis of the annual mass balance series using all available data and
following a methodology based on Zemp et al. (2013) is intended, but beyond the scope of this paper.

We found that avalanches contributed at least 0.31 m w.e. to the winter mass balance of 2018 and 0.55 m w.e. to the multiyear
275 geodetic mass balance. We hypothesize, that the difference between these two values i.e. the larger contribution of avalanches
on the multiyear geodetic mass balance could be attributed to 1) systematically higher snow densities within the avalanche
deposits of 2018, 2) reduced melt rates at the avalanche deposits due to an increased albedo and 3) to enhanced internal
accumulation and reduced runoff within the firn layer of the avalanche deposits as discussed before.

280 Regardless of the recent uncertainty in the glaciological time series of FG there is a shift from rather negative to less negative
mass balances with 2013/2014 which we attribute to higher winter accumulation between 2014 and 2018. This shift to less
negative mass balances - caused by an increase in precipitation over NE Greenland in recent years – has been shown to be a
regional effect by Hugonnet et al. (2021) and by Khan et al. (2022).



285 6 Conclusions

Our study shows that the 8-year geodetic mass balance 2013/14 -2020/21 of FG has been slightly positive. A significant positive contribution to the mass balance originates from widespread avalanche depositions from the surrounding slopes in February 2018, which affected more than one third of the glacier area. We estimated the contribution of avalanches to the winter mass balance of 2018 as 0.31 m w.e. at least and the contribution to the cumulative 8-year geodetic mass balance as 0.55 m w.e. We showed that the 8-year geodetic mass balance of Freya Glacier would have been negative without the contribution from snow avalanches. A main uncertainty in this assessment is introduced by a lack of snow and firn density measurements especially within the avalanche depositions, but also in the upper firn areas. Measurements of firn density should receive more priority in the future mass balance monitoring of FG. The cumulative glaciological mass balance suffers from data gaps and only a few point observations in recent years and underestimates the mass balance significantly. As FG is surrounded by steep slopes, we assume that accumulation from avalanches might have contributed also in the past, but 2018 was the first and only time since the beginning of the monitoring in 2007, that avalanches have been observed widespread over the glacier area. Assuming a higher likelihood of strong winter precipitation events in a warmer climate, we expect that accumulation by avalanches might become more important on Arctic mountain glaciers that are situated in or surrounded by steep terrain.

300

Data availability

All raw data can be provided by the corresponding author upon request.

305

Author Contributions

BH designed the study, conducted the data analysis and wrote the manuscript. BH, DB carried out the geodetic surveys. BH, DB, MC, SHL, JA and WS carried out mass balance observations on Freya Glacier. DB analysed the GPR data. GV helped with planning and processing of the 2013 geodetic survey. WS and EL provided the funding. All authors provided insights regarding the interpretation of data and reviewed and edited the manuscript.

310

The authors declare that they have no conflict of interest.

Acknowledgements

The work is supported by the International School for Alpine Research at Sonnblick Observatory (ISAR-SBO), a research Grant from GeoSphere Austria. The survey in 2013 was supported by Österreichische Gesellschaft für Polarforschung. Data from the Greenland Ecosystem Monitoring Programme were provided by Asiaq – Greenland Survey, Nuuk, Greenland. The authors are grateful to the logistics team at Zackenberg Research Station for the logistical support of the fieldwork. The authors gratefully acknowledge Geo Boffi for processing of the GNSS data of 2013.

320



References

- Abermann, J., Eckerstorfer, M., Malnes, E., and Hansen, B. U.: A large wet snow avalanche cycle in West Greenland quantified using remote sensing and in situ observations, *Nat Hazards*, 97, 517–534, <https://doi.org/10.1007/s11069-019-03655-8>, 2019a.
- 325 Abermann, J., Van As, D., Wacker, S., Langley, K., Machguth, H., and Fausto, R. S.: Strong contrast in mass and energy balance between a coastal mountain glacier and the Greenland ice sheet, *J. Glaciol.*, 65, 263–269, <https://doi.org/10.1017/jog.2019.4>, 2019b.
- AgiSoft LLC (2023):, 2023.
- Ahlmann, H. W.: Studies in Northeast Greenland: Part III: Accumulation and Ablation on the Frøya Glacier: Its Regime in 1938-39 and in 1939-40, *Geografiska Annaler*, 24, 1–22, 1942.
- 330 Ahlmann, H. W.: The Frøya Glacier 1939-40: Accumulation and Ablation on the Frøya Glacier, *Geografiska Annaler*, 28, 239–257, 1946.
- Binder, D., Schöner, W., Brückl, E., Hynek, B., and Weyss, G.: Ground Penetrating Radar Investigations in the North East of Greenland, in: *Geophysical Research Abstracts*, EGU General Assembly 2009, Wien, 2009.
- 335 Braithwaite, R. J., Laternser, M., and Pfeffer, W. T.: Variations of near-surface firn density in the lower accumulation area of the Greenland ice sheet, Pâkitsoq, West Greenland, *J. Glaciol.*, 40, 477–485, <https://doi.org/10.3189/S002214300001234X>, 1994.
- Citterio, M. and Ahlstrøm, A. P.: The GlacioBasis glacier monitoring programme at A.P. Olsen Ice Cap (Zackenbergl, NE Greenland), in: *Nordic Glaciology. Abstract from Glaciological Society Nordic Branch Meeting, 28-30 October 2010*, Copenhagen, 2010.
- 340 Citterio, M. and Ahlstrøm, A. P.: The GlacioBasis glacier monitoring programme at A.P. Olsen Ice Cap (Zackenbergl, NE Greenland), in: *Nordic Glaciology. Abstract from Glaciological Society Nordic Branch Meeting, 28-30 October 2010*, Copenhagen, 2010.
- Fausto, R. S., Van As, D., Mankoff, K. D., Vandecrux, B., Citterio, M., Ahlstrøm, A. P., Andersen, S. B., Colgan, W., Karlsson, N. B., Kjeldsen, K. K., Korsgaard, N. J., Larsen, S. H., Nielsen, S., Pedersen, A. Ø., Shields, C. L., Solgaard, A. M., and Box, J. E.: Programme for Monitoring of the Greenland Ice Sheet (PROMICE) automatic weather station data, *Earth Syst. Sci. Data*, 13, 3819–3845, <https://doi.org/10.5194/essd-13-3819-2021>, 2021.
- 345 Frederikse, T., Landerer, F., Caron, L., Adhikari, S., Parkes, D., Humphrey, V. W., Dangendorf, S., Hogarth, P., Zanna, L., Cheng, L., and Wu, Y.-H.: The causes of sea-level rise since 1900, *Nature*, 584, 393–397, <https://doi.org/10.1038/s41586-020-2591-3>, 2020.
- Geissler, J., Mayer, C., Jubanski, J., Münzer, U., and Siegert, F.: Analyzing glacier retreat and mass balances using aerial and UAV photogrammetry in the Ötztal Alps, Austria, *The Cryosphere*, 15, 3699–3717, <https://doi.org/10.5194/tc-15-3699-2021>, 2021.
- 350 Gindraux, S., Boesch, R., and Farinotti, D.: Accuracy Assessment of Digital Surface Models from Unmanned Aerial Vehicles' Imagery on Glaciers, *Remote Sensing*, 9, 186, <https://doi.org/10.3390/rs9020186>, 2017.
- Hugonnet, R., McNabb, R., Berthier, E., Menounos, B., Nuth, C., Girod, L., Farinotti, D., Huss, M., Dussaillant, I., Brun, F., and Kääh, A.: Accelerated global glacier mass loss in the early twenty-first century, *Nature*, 592, 726–731, <https://doi.org/10.1038/s41586-021-03436-z>, 2021.
- 355 Huss, M.: Density assumptions for converting geodetic glacier volume change to mass change, *The Cryosphere*, 7, 877–887, <https://doi.org/10.5194/tc-7-877-2013>, 2013.
- Huss, M., Bauder, A., and Funk, M.: Homogenization of long-term mass-balance time series, *Ann. Glaciol.*, 50, 198–206, <https://doi.org/10.3189/172756409787769627>, 2009.
- 360 Hynek, B., Weyss, G., Binder, D., Schöner, W., Abermann, J., and Citterio, M.: Mass balance of Freya Glacier, Greenland since 2007/2008, , <https://doi.org/10.1594/PANGAEA.831035>, 2014.
- Hynek, B., Binder, D., and Citterio, M.: The Mass balance of Freya Glacier, Greenland, in 2015/2016. Technical Document, ZAMG, 2018.



- Freya Glacier Webcam 1: <https://www.foto-webcam.eu/webcam/freya1/>, last access: 6 October 2023.
- 365 Freya Glacier Webcam 2: <https://www.foto-webcam.eu/webcam/freya2/>, last access: 6 October 2023.
- Kaser, G., Fountain, A., and Jansson, P.: A manual for monitoring the mass balance of mountain glaciers, 2003.
- Khan, S. A., Colgan, W., Neumann, T. A., van den Broeke, M. R., Brunt, K. M., Noël, B., Bamber, J. L., Hassan, J., and Bjørk, A. A.: Accelerating Ice Loss From Peripheral Glaciers in North Greenland, *Geophysical Research Letters*, 49, <https://doi.org/10.1029/2022GL098915>, 2022.
- 370 Klug, C., Bollmann, E., Galos, S. P., Nicholson, L., Prinz, R., Rieg, L., Sailer, R., Stötter, J., and Kaser, G.: Geodetic reanalysis of annual glaciological mass balances (2001–2011) of Hintereisferner, Austria, *The Cryosphere*, 12, 833–849, <https://doi.org/10.5194/tc-12-833-2018>, 2018.
- Laha, S., Kumari, R., Singh, S., Mishra, A., Sharma, T., Banerjee, A., Nainwal, H. C., and Shankar, R.: Evaluating the contribution of avalanching to the mass balance of Himalayan glaciers, *Ann. Glaciol.*, 58, 110–118, <https://doi.org/10.1017/aog.2017.27>, 2017.
- 375 Larsen, S. H., Rutishauser, A., Binder, D., Korsgaard, N., Hynek, B., and Citterio, M.: Glaciological monitoring at A. P. Olsen Ice Cap in NE Greenland, oral, <https://doi.org/10.5194/egusphere-egu23-15647>, 2023.
- Li, X., Sovilla, B., Jiang, C., and Gaume, J.: Three-dimensional and real-scale modeling of flow regimes in dense snow avalanches, *Landslides*, 18, 3393–3406, <https://doi.org/10.1007/s10346-021-01692-8>, 2021.
- 380 Machguth, H., MacFerrin, M., Van As, D., Box, J. E., Charalampidis, C., Colgan, W., Fausto, R. S., Meijer, H. A. J., Mosley-Thompson, E., and Van De Wal, R. S. W.: Greenland meltwater storage in firn limited by near-surface ice formation, *Nature Clim Change*, 6, 390–393, <https://doi.org/10.1038/nclimate2899>, 2016a.
- Machguth, H., Thomsen, H. H., Weidick, A., Ahlstrøm, A. P., Abermann, J., Andersen, M. L., Andersen, S. B., Bjørk, A. A., Box, J. E., Braithwaite, R. J., Bøggild, C. E., Citterio, M., Clement, P., Colgan, W., Fausto, R. S., Gleie, K., Gubler, S., Hasholt, B., Hynek, B., Knudsen, N. T., Larsen, S. H., Mernild, S. H., Oerlemans, J., Oerter, H., Olesen, O. B., Smeets, C. J. P. P., Steffen, K., Stober, M., Sugiyama, S., Van As, D., Van Den Broeke, M. R., and Van De Wal, R. S. W.: Greenland surface mass-balance observations from the ice-sheet ablation area and local glaciers, *Journal of Glaciology*, 62, 861–887, <https://doi.org/10.1017/jog.2016.75>, 2016b.
- 385
- 390 Marcer, M., Stentoft, P. A., Bjerre, E., Cimoli, E., Bjørk, A., Stenseng, L., and Machguth, H.: Three Decades of Volume Change of a Small Greenlandic Glacier Using Ground Penetrating Radar, Structure from Motion, and Aerial Photogrammetry, *Arctic, Antarctic, and Alpine Research*, 49, 411–425, <https://doi.org/10.1657/AAAR0016-049>, 2017.
- Mernild, S. H., Pelto, M., Malmros, J. K., Yde, J. C., Knudsen, N. T., and Hanna, E.: Identification of snow ablation rate, ELA, AAR and net mass balance using transient snowline variations on two Arctic glaciers, *J. Glaciol.*, 59, 649–659, <https://doi.org/10.3189/2013JoG12J221>, 2013.
- 395 Noël, B., Aðalgeirsdóttir, G., Pálsson, F., Wouters, B., Lhermitte, S., Haacker, J. M., and van den Broeke, M. R.: North Atlantic Cooling is Slowing Down Mass Loss of Icelandic Glaciers, *Geophysical Research Letters*, 49, <https://doi.org/10.1029/2021GL095697>, 2022.
- Nuth, C. and Kääb, A.: Co-registration and bias corrections of satellite elevation data sets for quantifying glacier thickness change, *The Cryosphere*, 5, 271–290, <https://doi.org/10.5194/tc-5-271-2011>, 2011.
- 400 Østrem, G. and Brugmann, M.: *Glacier Mass Balance Measurements. A manual for field and office work.*, National Hydrology Research Institute (Canada), 1991.
- Piermattei, L., Carturan, L., and Guarnieri, A.: Use of terrestrial photogrammetry based on structure-from-motion for mass balance estimation of a small glacier in the Italian alps: SfM-MVS APPROACH FOR GLACIER MASS BALANCE ESTIMATION, *Earth Surf. Process. Landforms*, 40, 1791–1802, <https://doi.org/10.1002/esp.3756>, 2015.
- 405 Rastner, P., Bolch, T., Mölg, N., Machguth, H., Le Bris, R., and Paul, F.: The first complete inventory of the local glaciers and ice caps on Greenland, *The Cryosphere*, 6, 1483–1495, <https://doi.org/10.5194/tc-6-1483-2012>, 2012.

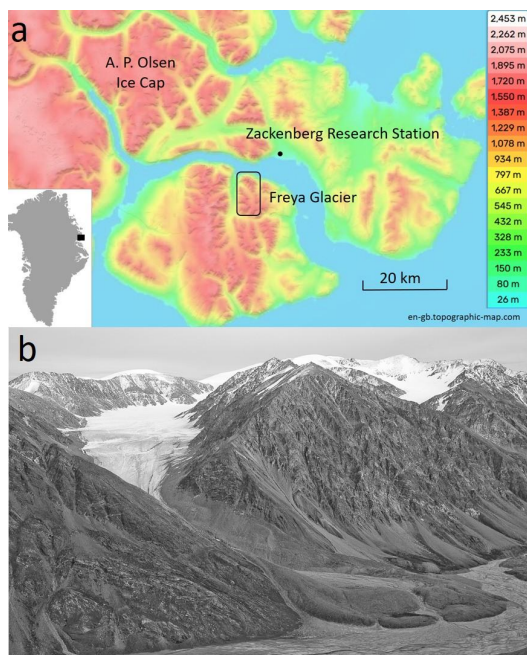


- Rossini, M., Di Mauro, B., Garzonio, R., Baccolo, G., Cavallini, G., Mattavelli, M., De Amicis, M., and Colombo, R.: Rapid melting dynamics of an alpine glacier with repeated UAV photogrammetry, *Geomorphology*, 304, 159–172, <https://doi.org/10.1016/j.geomorph.2017.12.039>, 2018.
- 410 Schmidt, N. M., Reneerkens, J., Christensen, J. H., Olesen, M., and Roslin, T.: An ecosystem-wide reproductive failure with more snow in the Arctic, *PLoS Biol*, 17, e3000392, <https://doi.org/10.1371/journal.pbio.3000392>, 2019.
- Schöner, W., Binder, D., Hynek, B., Weyss, G., Abermann, J., Olefs, M., and Nicus, U.: Climate change and glacier reaction in Zackenberg Region, National Environmental Research Institute, Aarhus University, Denmark, 2009.
- 415 Sovilla, B., Somnavilla, F., and Tomaselli, A.: Measurements of mass balance in dense snow avalanche events, *Ann. Glaciol.*, 32, 230–236, <https://doi.org/10.3189/172756401781819058>, 2001.
- Turchaninova, A., Sokratov, S., Seliverstov, Y., Petrakov, D., Lazarev, A., and Bashkova, E.: Non-climatic factors affecting glacier mass balance (on the example of avalanche nourishment), oral, <https://doi.org/10.5194/egusphere-egu2020-18937>, 2020.
- 420 Vandecrux, B., Fausto, R. S., Langen, P. L., Van As, D., MacFerrin, M., Colgan, W. T., Ingeman-Nielsen, T., Steffen, K., Jensen, N. S., Møller, M. T., and Box, J. E.: Drivers of Firn Density on the Greenland Ice Sheet Revealed by Weather Station Observations and Modeling, *JGR Earth Surface*, 123, 2563–2576, <https://doi.org/10.1029/2017JF004597>, 2018.
- WGMS: Glacier Mass Balance Bulletin No. 12 (2010-2011), edited by: Zemp, M., Nussbaumer, S. U., Naegeli, K., Gärtner-Roer, I., F. P., Hoelzle, M., and Haerberli, W., ICSU (WDS) / IUGG (IACS) / UNEP / UNESCO / WMO / World Glacier Monitoring Service, Zurich, Switzerland, 106 pp., 2013.
- 425 World Glacier Monitoring Service (WGMS): Fluctuations of Glaciers Database (wgms-fog-2022-09), <https://doi.org/10.5904/WGMS-FOG-2022-09>, 2022.
- Yde, J. C., Gillespie, M. K., Løland, R., Ruud, H., Mernild, S. H., Villiers, S. D., Knudsen, N. T., and Malmros, J. K.: Volume measurements of Mittivakkat Gletscher, southeast Greenland, *J. Glaciol.*, 60, 1199–1207, <https://doi.org/10.3189/2014JG14J047>, 2014.
- 430 Zemp, M., Thibert, E., Huss, M., Stumm, D., Rolstad Denby, C., Nuth, C., Nussbaumer, S. U., Moholdt, G., Mercer, A., Mayer, C., Joerg, P. C., Jansson, P., Hynek, B., Fischer, A., Escher-Vetter, H., Elvehøy, H., and Andreassen, L. M.: Reanalysing glacier mass balance measurement series, *The Cryosphere*, 7, 1227–1245, <https://doi.org/10.5194/tc-7-1227-2013>, 2013.
- 435 Zemp, M., Huss, M., Thibert, E., Eckert, N., McNabb, R., Huber, J., Barandun, M., Machguth, H., Nussbaumer, S. U., Gärtner-Roer, I., Thomson, L., Paul, F., Maussion, F., Kutuzov, S., and Cogley, J. G.: Global glacier mass changes and their contributions to sea-level rise from 1961 to 2016, *Nature*, 568, 382–386, <https://doi.org/10.1038/s41586-019-1071-0>, 2019.

440



Figures and Tables:



445

Figure 1: a) Location of Freya (Freja) Glacier (74.38°N, 20.82°E) on Clavering Island in Northeast Greenland, next to Zackenberg Research Station and A.P. Olsen Icecap. (Map from en-gb.topographic-map.com) b) Foto of Freya Glacier and its surrounding ridges in August 2008 (Foto: B. Hynek).

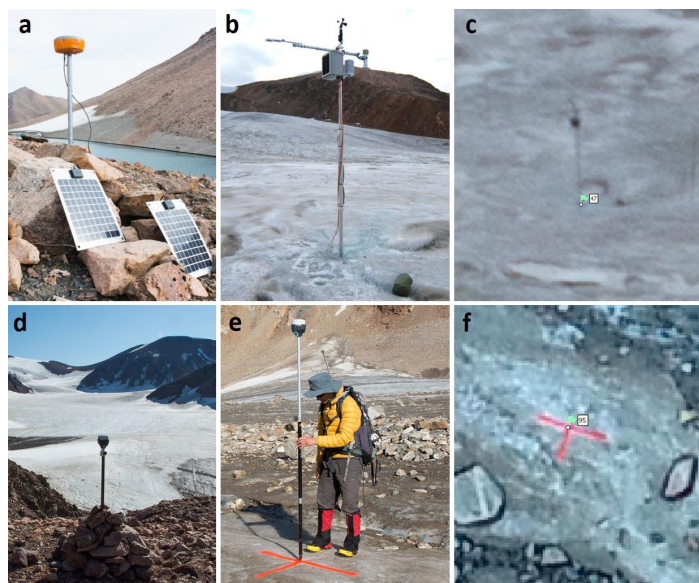


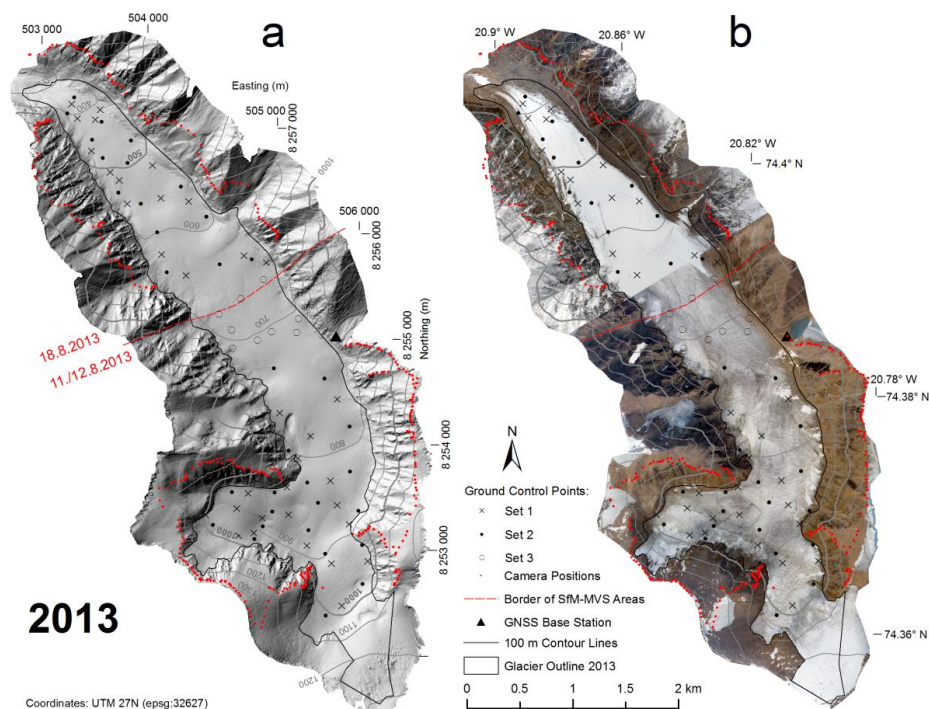
Figure 2: Upper panel: GNSS Survey 2013. a) GNSS base station b) example of a natural GCP and c) its visibility in the imagery. Lower panel: GNSS Survey of 2021. d) GNSS Base Station e) Survey of an artificial GCP and f) its visibility of the GCP in the imagery.

450

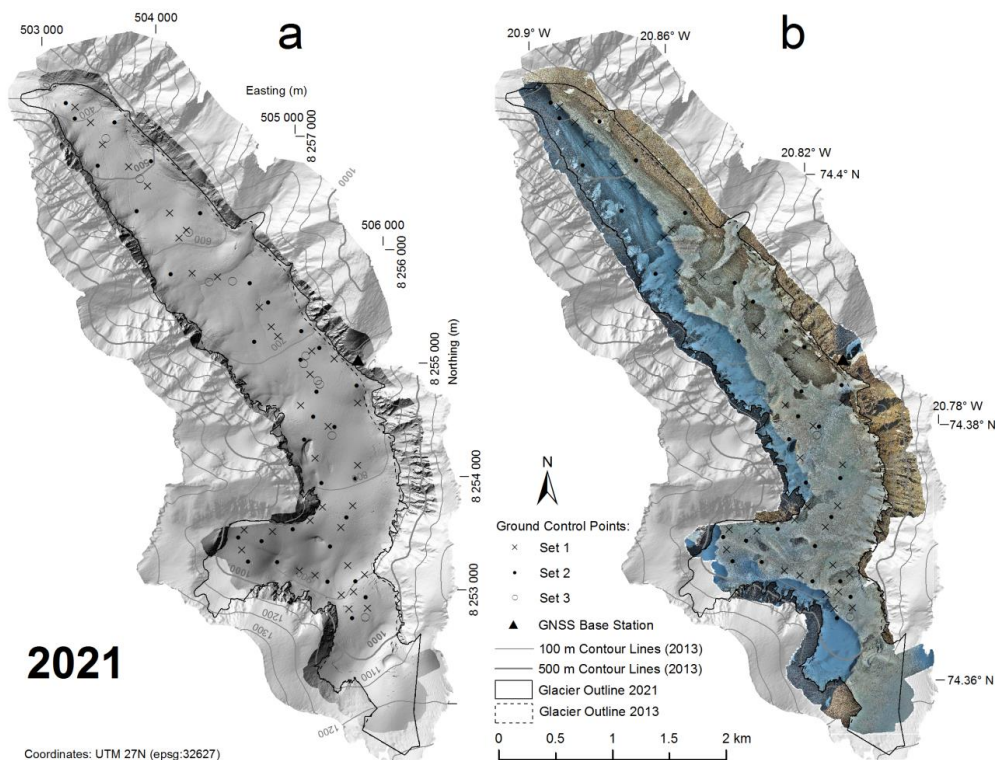


Table 1: Main characteristics of the two SfM-MVS surveys.

	2013	2021
Survey dates	11. - 18.8.2013	27.-31.7.2021
Survey Geometry	Oblique (Terrestrial)	Nadir (UAV)
Camera/UAV	Nikon D7100 + 20mm	Phantom 4 RTK
Image Resolution	24 Mpix	20 Mpix
No of Images	430	6250
Height above glacier surface	10 - 400	140
Ground Sampling Distance	> 20 cm	3.8 cm
No. of visible GCPs	67	68
Density of visible GCPs [/km ²]	12.6	13.6
Max. elevation change during survey [m]	< 0.15	< 0.20
Surface reconstruction [% of Glacier Area]	100%	94%
DEM spatial resolution [m]	1	0.2
Orthophoto spatial resolution [m]	0.25	0.05



455 **Figure 3:** a) Hillshade of the resulting DEM 2013 in 1m resolution and b) Orthophoto of the survey in August 2013. On both maps the locations of the photo points, the ground control points (GCPs) and the GNSS Base Station are indicated. The upper part of the glacier was surveyed on 11.8. and 12.8. The lower part of the glacier was surveyed on 18.8. after a snow fall event that marked the end of the ablation season in 2013.



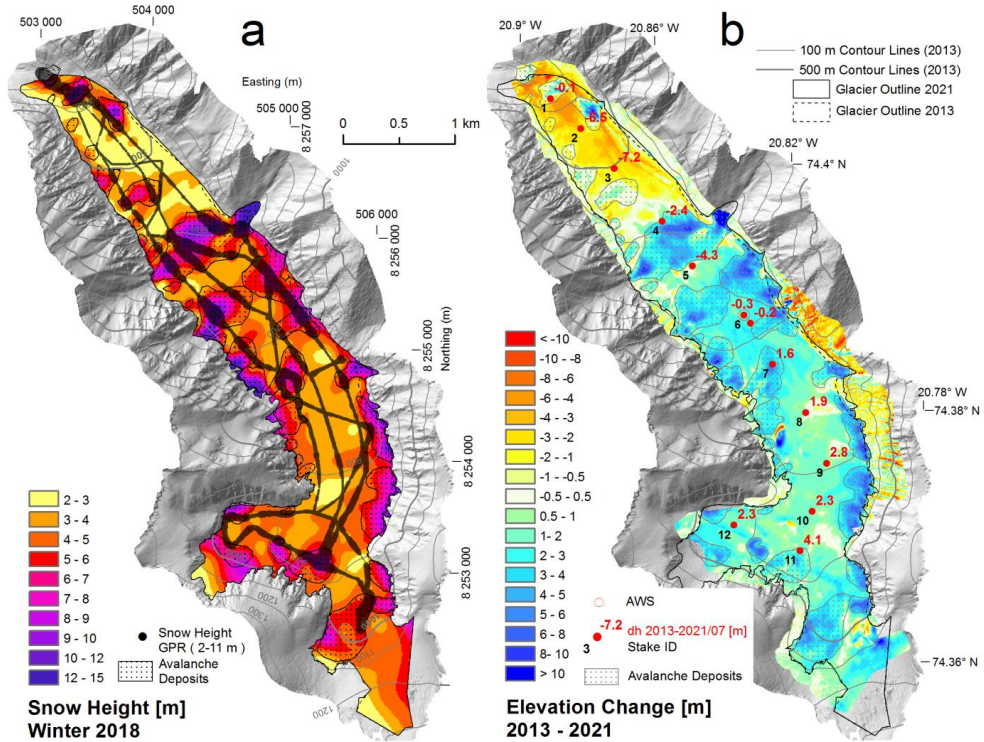
460

Figure 4: a) Hillshade of the 2021 DEM (dark grey) in 1m resolution and b) Orthophoto of the survey in July 2021. On both maps the hillshade of 2013 is displayed in the background and the locations of the ground control points (GCPs) and the GNSS base station are indicated. The lower part of the glacier was photographed on 27.7.2021 and the upper part on 31.7 2021.

465

Table 2: Error statistics of the ground control points in both sfm-models

Model	No of Control Points (Set 2)	RMSE Control Points [m]				No of Check Points (Set 1)	RMSE Check Points [m]				No of z-Val Points (Set 3)	RMSE [m] Z
		X	Y	Z	TOT		X	Y	Z	TOT		
2013	33	0.14	0.12	0.10	0.21	32	0.41	0.37	0.20	0.59	9	0.37
2021	31	0.20	0.10	0.16	0.28	36	0.21	0.10	0.18	0.30	11	0.12



470 **Figure 5:** a) Measured (GPR) and extrapolated snow height in winter 2018 and delineation of avalanche affected areas. b) Elevation Change between 18.8.2013 and 27.7.2021 and stake/AWS locations.

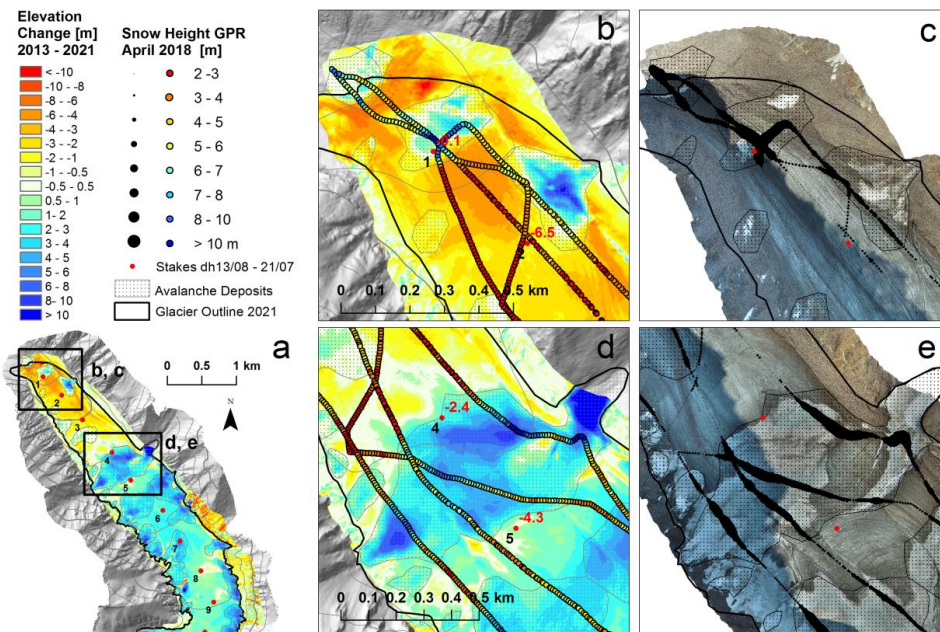
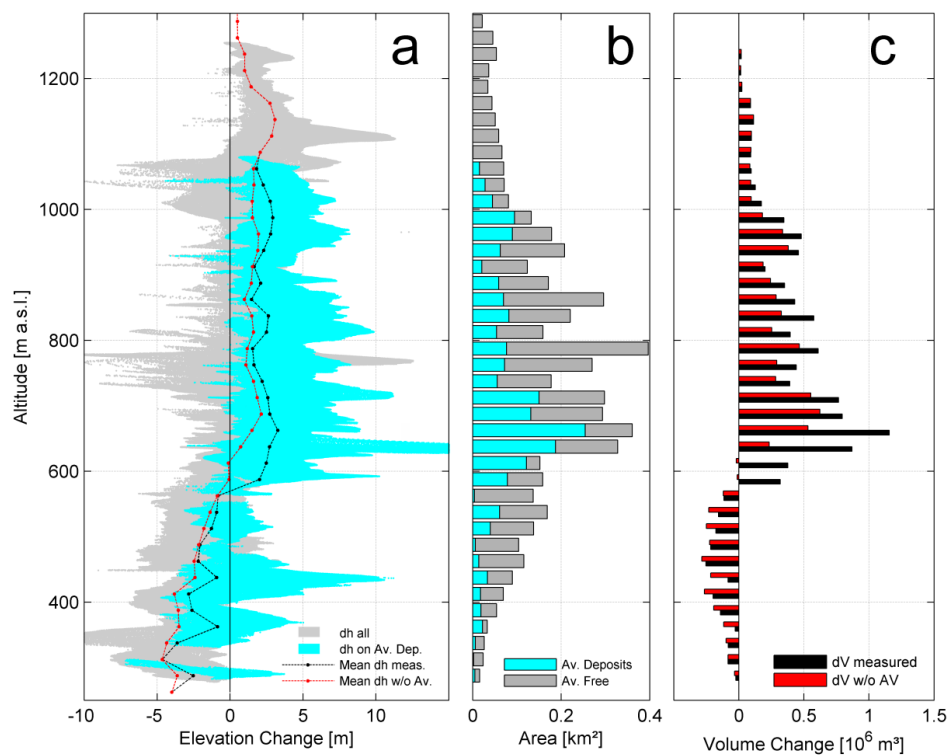


Figure 6: a) Overview and (b, d) close-ups of Elevation Changes and (c, e) Orthophoto 2021 together with GPR snow height data of spring 2018 and measured ablation at the stakes.

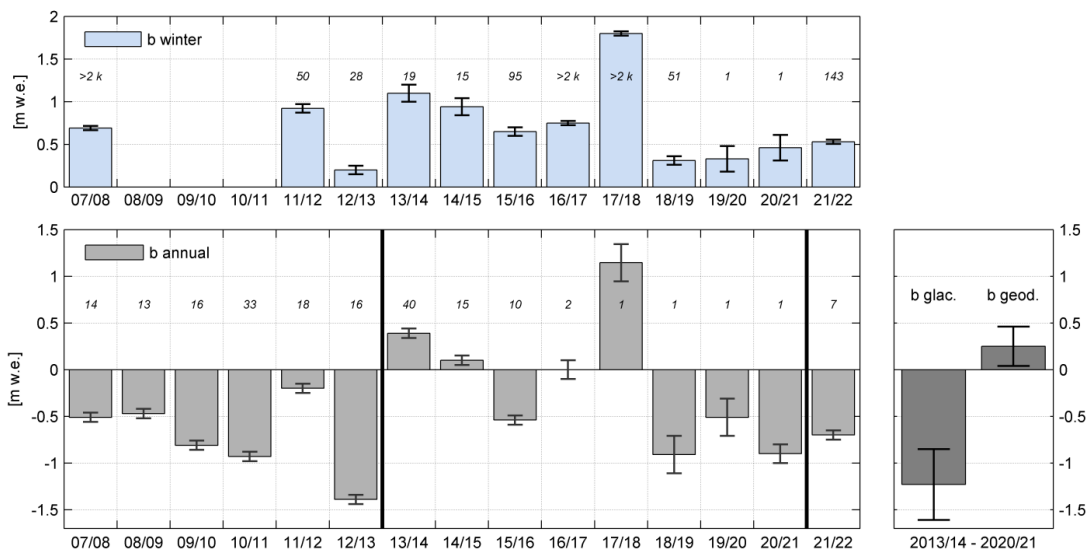


475 **Table 3:** Spatial mean values of the winter balance 2018 and the multiyear geodetic mass balance.

	Spatial Mean on Total Glacier Area	Spatial Mean on Glacier Area affected by avalanches 2018	Spatial Mean on Glacier Area NOT affected by avalanches 2018
Surface Area 2021 [km ²]	5.54	1.98	3.55
Surface Area [%]	100%	36%	64%
Elevation change [m] 08/2013 - 07/2021	1.56 ± 0.15	3.18	0.67
Geod. mass balance [m w.e.] 08/2013 - 07/2021	0.85 ± 0.20	1.92	0.26
Winter 2018 snow height [m]	4.79	6.24	4.00
Winter mass balance [m w.e.] (same density)	1.85	2.40	1.54



480 **Figure 7:** a) Altitudinal distribution of elevation change values on 1 m grid resolution, in cyan values on avalanche influenced areas and mean values on 25 m elevation bins of all grid cells (black) and grid cells without avalanche influence. b) glacier area on elevation bins and c) calculated volume changes (dV) and hypothetical dV without avalanches.



485

Figure 8: Left panels: Time series of specific winter mass balances (top), and specific annual mass balances (bottom) with their estimated uncertainties. The number of point observations available for the mass balance calculation of individual years (winters) is shown as italic numbers. E.g. winter mass balance 2017/18 is based on more than 2000 point observations, while annual balance 2017/18 is based on one point observation only. Right panel: Comparison of the cumulative glaciological and geodetic mass balance 2013/14 – 2020/21 and their related uncertainties.

490